Int J Mech Mater Des (2018) 14:91–104
https://doi.org/10.1007/s10999-016-9362-1

Surface effect on dynamic stability of microcantilevers on an elastic foundation under a subtangential follower force

X.-F. Li · S.-N. Jiang · K. Y. Lee

Received: 27 July 2016 / Accepted: 22 December 2016 / Published online: 30 December 2016

Abstract For micro/nano structures, surface elasticity, surface stress and surface mass strongly affect mechanical behaviors of 1D beam-columns. This article studies dynamic stability of microcantilevers on an elastic foundation or embedded in an elastic matrix when subjected to a subtangential follower force, where the surface effects are taken into account. An exact characteristic equation is derived for clamped–free end supports. For differential tangency coefficients, the force–frequency interaction diagram is displayed and the influences of surface elasticity modulus, residual surface tension, surface mass and the elastic foundation are analyzed for conservative and non-conservative compressive forces. When the tangency coefficient vanishes, a cantilever column subjected to a conservative tip force is reduced, and conventional Euler buckling for a compressive axial load is recovered. When the tangency coefficient does not vanish, a generalized Beck's column with the surface effects is tackled. When the tangency coefficient exceeds certain critical value, flutter instability take places. For a fixed frequency, the critical divergency and flutter loads as a function of the tangency coefficient are given for various surface influences from residual surface tension, surface elasticity, surface mass and the stiffness of the elastic foundation. The boundary map of stability, divergence and flutter domain is shown.

Keywords Dynamic stability · Flutter load · Surface stress · Surface elasticity · Surface mass · Elastic foundation

1 Introduction

With the development of micro/nano technique, one-dimensional (1D) beam-like micro/nanoscale structures have a wide application in MEMS/NEMS such as sensors, AFMs, etc. Due to their very large aspect ratio, such 1D micro/nano structures have apparent size-dependent material properties, which is completely different from conventional 1D structures. Since their diameter falls into the order of micro/nanometer, the size effects, in particular surface effects, are noticeable and they cannot be simply neglected in assessing their mechanical behaviors. The surface effects, in turn, can strongly affect material properties of a small scale solid, and the surface effects have been recognized as a key factor responsible for experimentally measured size-dependent mechanical

X.-F. Li · S.-N. Jiang
School of Civil Engineering, Central South University, Changsha 410075, People's Republic of China

X.-F. Li · K. Y. Lee (✉)
State Key Laboratory of Structural Analysis for Industrial Equipment and Department of Engineering Mechanics, Dalian University of Technology, Dalian 116024, People's Republic of China
e-mail: kylee@dlut.edu.cn

properties. Along this line, great progress has been made to show the influence of the surface stress as well as surface elasticity on mechanical behaviors.

From this viewpoint, much theoretical and experimental attention has been directed towards the investigation of the surface effects. Cuenot et al. (2004) applied resonant-contact atomic force microscopy to measure the elastic properties of silver and lead nanowires and found that the increase of apparent elastic modulus for smaller diameters is attributed to surface tension effects. A large number of theoretical papers related to the surface effects have been reported to interpret how the surface stress and surface elasticity affect the mechanical behaviors of micro or nanobeams. By analyzing microcantilever beams, the surface stress was suggested to account for change in the natural frequency (McFarland et al. 2005). When a nanomechanical cantilever is immersed in a viscous fluid, the dynamic response of frequency shift due to the surface stress was studied (Dorignac et al. 2006). Also the effect of surface stress on the stiffness of a cantilever plate has been formulated based on a three-dimensional model (Lachut and Sader 2007), where surface stress difference and the corresponding couple are ignored. For other static bending of a microscale beam with the surface stress, three typical theoretical models for a beam with rectangular cross section have been presented by Zhang et al. (2004). The response bending of a beam with arbitrary cross section on the surface stress was also treated (Li and Peng 2008).

On the other hand, within the framework of surface elasticity (Gurtin and Murdoch 1975), great progress has been made in characterizing the mechanical properties of micro/nano solids and structures with consideration of the surface stress incorporating surface elasticity (Dingreville et al. 2005). Wang et al. (2011) commented relevant work before 2011 in a review article. The dependence of effective bending stiffness of a nanobeam or nanoplate on the surface stress and surface elasticity was expounded through the atomic simulations (Miller and Shenoy 2000). Yi and Duan (2009) established a quantitative relation between continuum-level descriptions of surface stress and molecular-level descriptions via the van der Waals and Coulomb interactions. Wang et al. (2013) derived a relation between the surface stress and stress intensity factors based on the classical linear fracture mechanics. In particular, using the surface stress together with surface elasticity, the static bending of a nanowire has been dealt with based on the Euler–Bernoulli theory (He and Lilley 2008b; Liu and Rajapakse 2010) and the Timoshenko theory (He and Lilley 2012; Li et al. 2014; Nazemnezhad and Hosseini-Hashemi 2015). For dynamic response within the framework of the Euler–Bernoulli theory, transverse vibration of nanomechanical cantilevers has been investigated by Wang and Feng (2007) and He and Lilley (2008a). When considering the shear deformation and rotational moment of inertia of cross-section, free vibration (Wang and Feng 2009; Farshi et al. 2010) and forced vibration (Wu et al. 2016) of a small scale beam were analyzed. Using various beam theories, governing equations were established and buckling and vibration analyses of a nanobeam-column with the surface effects were coped with by Ansari et al. (2014). Adopting the nonlocal beam theory incorporating the surface effect, some analyses on free vibration and buckling of nanowires have been made (Lee and Chang 2010; Elishakoff and Soret 2013; Hosseini-Hashemi et al. 2015; Attia and Mahmoud 2016). For fluid-conveying nanotubes with consideration of surface effects, vibration characteristic and dynamic response were formulated (Wang 2010; Zhang and Meguid 2016). Furthermore, The effect of high-order surface stress on buckling and vibration behavior of nanowires (Chiu and Chen 2012, 2013; Zhang et al. 2015). Chen and Chiu (2011) also analyzed the effect of higher-order interface stresses on mechanical behavior of two-dimensional composites. A Timoshenko beam model incorporating microstructure and surface energy effects has been set forth by Gao (2015). As a mass sensor, Agwa and Eltaher (2016) analyzed the effect of surface stress on vibrational frequencies. A general model of nanocantilever switches was investigated with surface effects included (Wang and Wang 2015). The effect of magnetic field on vibration and buckling behavior of a current-carrying nanowire was treated by Kiani (2014, 2015). Some bending-based test methods for elastic modulus of nanowires when surface effects are taken into account have been suggested (Zheng et al. 2010; Qiao and Zheng 2013). Although a great amount of work has been conducted, there is little information on the study of dynamic stability of micro/nano beams with consideration of the surface effects. Very recently, Chen and Meguid (2015a, b, c, 2016) analyzed asymmetric bifurcation and snap-through

buckling behavior of initially curved microbeams. Li et al. (2016) studied flutter instability of a cantilever with tip mass and examined the influence of surface elasticity on flutter loads.

This paper aims at analyzing dynamic stability of microcantilevers when taking the surface effects into account. Under a generalized follower force at the free end, flutter instability of a microcantilever on an elastic foundation or embedded in a surrounding matrix is investigated in detail. An exact characteristic equation governing the force–frequency interaction relation is derived. The influences of surface elasticity, surface stress, surface mass, and the stiffness of elastic foundation on dynamic stability are shown graphically. The boundary of stability, divergence and flutter domains is presented.

2 Governing equations

Since the diameter of nanowires or microcantilevers falls down to the order of nano meter or micro meter, the surface effects are significant and cannot be simply neglected. Due to this reason, we consider dynamic stability of a microcantilever of length L subjected to a subtangential follower force P with tangency coefficient β at the free end, as shown in Fig. 1. The constitutive equations read

$$\sigma_{ij} = \lambda^B \varepsilon_{kk}\delta_{ij} + 2\mu^B \varepsilon_{ij}, \tag{1}$$

for the bulk material, and

$$\sigma^S_{\alpha\beta} = \sigma_0\delta_{\alpha\beta} + \left(\lambda^S + \sigma_0\right)\varepsilon^S_{\gamma\gamma}\delta_{\alpha\beta} + 2\left(\mu^S - \sigma_0\right)\varepsilon^S_{\alpha\beta} + \sigma_0 u^S_{\alpha,\beta}, \tag{2}$$

$$\sigma^S_{\alpha z} = \sigma_0 u^S_{z,\alpha}, \tag{3}$$

for the surface material (Gurtin and Murdoch 1975), where λ^B and μ^B are Lame constants, δ_{ij} the Kronecker delta, and σ_{ij} the stress components, ε_{ij} the strain components, $\varepsilon_{ij} = 0.5\left(u_{i,j} + u_{j,i}\right)$, u_j the displacement components, σ_0 is the residual surface tension under unconstrained conditions, which is equal to the preexisting initial surface energy, λ^S and μ^S the surface Lame constants independent of the residual surface tension. In the above, a quantity with the superscript S denotes the one for the surface material, and a comma in subscript denotes differentiation with respect to the coordinate following. For the present study, it is easy to find that the constitutive equations reduce to

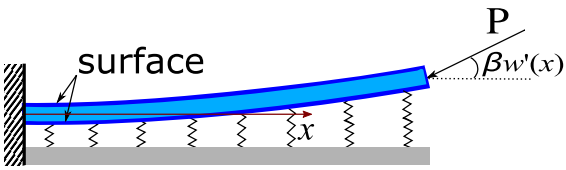

Fig. 1 Schematic of a microcantilever with consideration of surface effects when subjected to a subtangential follower force at the free end

$$\sigma = E\varepsilon, \tag{4}$$

for bulk material and

$$\sigma^s = \sigma_0 + E^s\varepsilon^s, \tag{5}$$

for surface material, where $\sigma\,(\varepsilon)$ and $\sigma^s\,(\varepsilon^s)$ are axial stress(strain) and axial surface stress (strain), E and E^s are moduli of bulk elasticity and surface elasticity, respectively. Note that both the surface stress and surface elastic modulus have the unit of Newton/meter, not Newton/meter^2. For flexural vibration or stability problems of slender microcantilevers, the Euler–Bernoulli beam hypothesis is suitable and adopted in the present paper. Hence according to this hypothesis, the axial strain can be expressed in terms of the deflection w as follows

$$\varepsilon = -z\kappa = -z\frac{\partial^2 w}{\partial x^2}, \tag{6}$$

where κ denotes the curvature of the deformed microcantilever, the x axis is orientated in the longitudinal direction, and the z axis is normal to the x axis upward.

The strain energy of a deformed microcantilever can be computed by

$$U = \frac{1}{2}\int_0^L \left(\int_A \sigma\varepsilon dA + \int_C \sigma^s\varepsilon^s ds\right)dx = \frac{D}{2}\int_0^L \left(\frac{\partial^2 w}{\partial x^2}\right)^2 dx, \tag{7}$$

with

$$D = EI + E^s J, \quad I = \int_A z^2 dA, \quad J = \int_C z^2 ds. \tag{8}$$

and the kinetic energy is calculated by

$$K = \frac{1}{2}\int_0^L \left[\int_A \rho\left(\frac{\partial w}{\partial t}\right)^2 dA + \int_C \rho^s \left(\frac{\partial w}{\partial t}\right)^2 ds\right] dx = \frac{m}{2}\int_0^L \left(\frac{\partial w}{\partial t}\right)^2 dx, \tag{9}$$

with

$$m = \rho A + \rho^s C, \tag{10}$$

where A is the cross-sectional area, C the corresponding boundary contour of the cross-section A.

In writing the above energy, we have neglected shear deformation and rotatory inertia of cross-section. In addition, when subjected to distributed lateral loading $q(x)$ over the whole microcantilever $0 < x < L$, and applied compressive subtangential follower force $P\,(P > 0)$ at the unsupported tip together with the residual surface tension, the total work done is

$$V = \int_0^L q(x)w(x)dx + \frac{1}{2}(P - H)\int_0^L \left(\frac{\partial w}{\partial x}\right)^2 dx, \tag{11}$$

where the small axial shortening prior to buckling has been ignored, and H stands for a resultant force due to the residual surface tension, i.e.

$$H = \int_C \sigma_0 ds. \tag{12}$$

In the above, small deformation and small rotation are assumed. If taking the residual surface tension as a constant, we find $H = 2(b + h)\sigma_0$ for rectangular cross-section with breadth b and height h, and $H = \pi\sigma_0 d$ circular cross-sections with diameter d. The results of H have a slight difference from those in He and Lilley (2008b).

We applies Hamilton's principle and substitute (7), (9) and (11) into the following equation

$$\delta\int_{t_1}^{t_2}(U - V - K)dt + \int_{t_1}^{t_2}\delta V^* dt = 0, \tag{13}$$

where V^* denotes the work at the free end done by the vertical (i.e. nonconservative) component of the subtangential follower force with the tangency coefficient β,

$$\delta V^* = \beta P \left.\frac{\partial w}{\partial x}\right|_{x=L} \delta w|_{x=L}, \tag{14}$$

where β is a tangency coefficient larger than or equal to zero. After performing variational operation we get the following governing partial differential equation

$$D\frac{\partial^4 w}{\partial x^4} + (P - H)\frac{\partial^2 w}{\partial x^2} + m\frac{\partial^2 w}{\partial t^2} = q(x), \tag{15}$$

and proper boundary conditions. Note that in this equation, the surface effects have been reflected through D, H, and m since D contains the contribution of the surface elasticity, H describes the contribution of the residual surface tension, and a part of m also accounts for the influence of the surface mass. For microcantilevers on an elastic foundation or embedded in a surrounding elastic matrix, the lateral loading q can be expressed in terms of $-Yw$, Y being the stiffness of the elastic foundation. Here the simplest Winkler foundation is used, although a general model such as Winkler–Pasternak foundation can be similarly solved without further difficulty.

For the problem in question, boundary conditions of a microcantilever subjected to a subtangential follower force at the free end in an angle $\beta\partial w/\partial x$ (Fig. 1) can be derived using Hamilton's principle and read

$$w = 0, \quad \frac{\partial w}{\partial x} = 0, \quad \text{at } x = 0, \tag{16}$$

$$\frac{\partial^2 w}{\partial x^2} = 0, \quad D\frac{\partial^3 w}{\partial x^3} + [P(1 - \beta) - H]\frac{\partial w}{\partial x} = 0, \quad \text{at } x = L, \tag{17}$$

It is noted that $\beta = 0$ corresponds to the case of the classical Euler–Bernoulli cantilever beam subjected to a conservative tip force along the horizontal direction, and $\beta = 1$ corresponds to the case of the usual follower force. The study on the case of $\beta = 0$ (i.e. Euler's column with the surface effects) has been reported in Wang and Feng (2007), while for other cases of $\beta > 0$, even for $\beta = 1$ (i.e. Beck's column with the surface effects), little information is available. It is worth pointing out that previous studies on vibration and stability of microcantilevers the surface effects do not contain surface mass, let along dynamic stability of microcantilevers.

3 Characteristic equation

In order to analyze bending vibration and structural stability of microcantilevers with the surface effects

subjected to a subtangential follower force, we take the deflection $w = W(\xi)e^{i\omega t}/L$ in (15) where $i = \sqrt{-1}$, $\xi = x/L$, W is the amplitude, and ω is the circular frequency. Thus, the governing Eq. (15) becomes

$$W^{IV} + \frac{p-\eta}{1+\lambda}W'' + \frac{k-(1+\mu)\Omega^2}{1+\lambda}W = 0, \tag{18}$$

where we have defined the following dimensionless quantities

$$p = \frac{PL^2}{EI}, \quad \eta = \frac{HL^2}{EI}, \quad \Omega^2 = \frac{\rho AL^4\omega^2}{EI}, \tag{19}$$

$$\lambda = \frac{E^sJ}{EI}, \quad \mu = \frac{\rho^sC}{\rho A}, \quad k = \frac{YL^4}{EI}, \tag{20}$$

and the prime denotes differentiation with respect to ξ. Using these dimensionless quantities, the boundary conditions (16) and (17) can be stated below

$$W(0) = 0, \quad W'(0) = 0, \tag{21}$$

$$W''(1) = 0, \quad W'''(1) + \frac{p(1-\beta)-\eta}{1+\lambda}W'(1) = 0. \tag{22}$$

If expressing a solution to Eq. (18) in the following form $W(\xi) = e^{\gamma\xi}$, one easily finds that the constant γ has to satisfy the following algebraic equation

$$\gamma^4 + \frac{p-\eta}{1+\lambda}\gamma^2 + \frac{k-(1+\mu)\Omega^2}{1+\lambda} = 0. \tag{23}$$

Solving the above algebraic equation one gets two pairs of distinct roots as $\pm\gamma_1$ and $\pm i\gamma_2$, where

$$\gamma_1 = \sqrt{\frac{\sqrt{(p-\eta)^2 + 4(1+\lambda)\left[(1+\mu)\Omega^2 - k\right]} - (p-\eta)}{2(1+\lambda)}}, \tag{24}$$

$$\gamma_2 = \sqrt{\frac{\sqrt{(p-\eta)^2 + 4(1+\lambda)\left[(1+\mu)\Omega^2 - k\right]} + (p-\eta)}{2(1+\lambda)}}. \tag{25}$$

Then a general solution to Eq. (18) is obtained to be

$$W = C_1\cosh(\gamma_1\xi) + C_2\sinh(\gamma_1\xi) + C_3\cos(\gamma_2\xi) + C_4\sin(\gamma_2\xi), \tag{26}$$

where $C_j (j = 1, 2, 3, 4)$ are unknown constants which do not vanish simultaneously.

Substituting (26) into the boundary conditions (21) and (22), after some manipulations, leads to

$$C_1 + C_3 = 0, \tag{27}$$

$$C_2\gamma_1 + C_4\gamma_2 = 0, \tag{28}$$

$$\gamma_1^2(C_1\cosh\gamma_1 + C_2\sinh\gamma_1) - \gamma_2^2(C_3\cos\gamma_2 + C_4\sin\gamma_2) = 0, \tag{29}$$

$$\gamma_1\left(\gamma_2^2 - \frac{p\beta}{1+\lambda}\right)(C_1\sinh\gamma_1 + C_2\cosh\gamma_1) + \gamma_2\left(\gamma_1^2 + \frac{p\beta}{1+\lambda}\right)(C_3\sin\gamma_2 - C_4\cos\gamma_2) = 0. \tag{30}$$

To gain a nontrivial solution of the above system of algebraic equations, the determinant of the coefficient matrix must be null,

$$\det\begin{bmatrix} 1 & 0 & 1 & 0 \\ 0 & \gamma_1 & 0 & \gamma_2 \\ \gamma_1^2\cosh\gamma_1 & \gamma_1^2\sinh\gamma_1 & -\gamma_2^2\cos\gamma_2 & -\gamma_2^2\sin\gamma_2 \\ \gamma_1\left(\gamma_2^2 - \frac{p\beta}{1+\lambda}\right)\sinh\gamma_1 & \gamma_1\left(\gamma_2^2 - \frac{p\beta}{1+\lambda}\right)\cosh\gamma_1 & \gamma_2\left(\gamma_1^2 + \frac{p\beta}{1+\lambda}\right)\sin\gamma_2 & -\gamma_2\left(\gamma_1^2 + \frac{p\beta}{1+\lambda}\right)\cos\gamma_2 \end{bmatrix} = 0, \tag{31}$$

which can be further simplified as

$$1+\frac{2(1+\lambda)\left[(1+\mu)\Omega^2-k\right]+(p-\eta)(p-\eta-p\beta)}{2(1+\lambda)\left[(1+\mu)\Omega^2-k\right]+(p-\eta)p\beta}\cosh\gamma_1\cos\gamma_2 - \frac{(p-\eta-2p\beta)\sqrt{(1+\lambda)\left[(1+\mu)\Omega^2-k\right]}}{2(1+\lambda)\left[(1+\mu)\Omega^2-k\right]+(p-\eta)p\beta}\sinh\gamma_1\sin\gamma_2=0. \tag{32}$$

In deriving the above equation, we have used the following relations:

$$\gamma_1^2+\gamma_2^2=\frac{\sqrt{(p-\eta)^2+4(1+\lambda)\left[(1+\mu)\Omega^2-k\right]}}{1+\lambda}, \tag{33}$$

$$\gamma_1^2-\gamma_2^2=-\frac{p-\eta}{1+\lambda}, \tag{34}$$

$$\gamma_1^2\gamma_2^2=\frac{(1+\mu)\Omega^2-k}{1+\lambda}. \tag{35}$$

Equation (32) is the characteristic equation we need to seek, which governs dynamic stability of a microcantilever on an elastic foundation or embedded in an elastic matrix subjected to a subtangential follower force at the free end. In particular, several special cases are mentioned as follows. When taking $p=0$, Eq. (32) gives the characteristic equation of free vibration of a microcantilever on an elastic foundation. When taking $\Omega=0$ and $\beta=0$, Eq. (32) gives the characteristic equation of buckling of a microcantilever subjected to a compressive force p. If $\beta=0$, Eq. (32) can be used to determine natural frequencies or buckling load for a microcantilever subject to a conservative force at the free end. In addition, if $\beta=1$, Eq. (32) in fact extends the classical Beck's column.

As a check, if setting $E^s=0, \rho^s=0$ and $\sigma_0=0$, implying the surface effects disappear, we find

$$\lambda=\mu=0,\quad \eta=0,\quad \gamma_1=\sqrt{\frac{\sqrt{p^2+4\left(\Omega^2-k\right)}-p}{2}}, \quad \gamma_2=\sqrt{\frac{\sqrt{p^2+4\left(\Omega^2-k\right)}+p}{2}}, \tag{36}$$

and the above characteristic equation (32) reduces to

$$1+\frac{2\left(\Omega^2-k\right)+p^2(1-\beta)}{2\left(\Omega^2-k\right)+p^2\beta}\cosh\gamma_1\cos\gamma_2 - \frac{p\left(\Omega^2-k\right)(1-2\beta)}{2\left(\Omega^2-k\right)+p^2\beta}\sinh\gamma_1\sin\gamma_2=0. \tag{37}$$

In the absence of surrounding matrix, i.e. $k=0$, the above result is in exact agreement with that derived in Zuo and Schreyer (1996). However, when considering the surface effects, the dynamic stability has an evident dependence on the surface elasticity, the residual surface tension, and surface mass, which can be seen from the characteristic equation (32).

4 Results and discussion

In this section, numerical calculations are carried out to examine the influence of surface effects on the dynamic stability of a microcantilever. For typical cross-section, we have

$$C=2(b+h),\quad A=bh,\quad I=\frac{1}{12}bh^3,\quad J=\frac{1}{2}bh^2+\frac{1}{6}h^3, \tag{38}$$

for rectangular cross-section with breadth b and height h, and

$$C=\pi d,\ A=\frac{1}{4}\pi d^2,\ I=\frac{1}{64}\pi d^4,\ J=\frac{1}{8}\pi d^3, \tag{39}$$

for circular cross-section with diameter d, respectively. Thus we get

$$\lambda=\frac{2E^s}{E}\left(\frac{3}{h}+\frac{1}{b}\right)(\text{for rec.})=\frac{8E^s}{Ed}(\text{for cir.}) \tag{40}$$

$$\mu=\frac{2\rho^s}{\rho}\left(\frac{1}{h}+\frac{1}{b}\right)(\text{for rec.})=\frac{4\rho^s}{\rho d}(\text{for cir.}) \tag{41}$$

Surface elasticity E^s may be positive or negative, depending on surface orientation, and its value covers a large range, e.g. taking -1170, -950 N/m (Gavan et al. 2009), -12.19, -10.655 N/m (Miller and Shenoy 2000), 1.22, -1.39 N/m (Shenoy 2005). Therefore, when diameter or height/breadth of cross-section of a microcantilever falls to the nano-meter

order, the influence of λ should be taken into account for usual bulk Young's modulus of 100 GPa order. In the following, we choose a material with properties $E = 56.25$ GPa, $v = 0.25$, $\rho = 3000\,\mathrm{kg/m^3}$ $E^s = 19.73$ KPa, $v^s = 0.233$, $\rho^s = 0.0007\,\mathrm{kg/m^3}$, $\sigma_0 = 110\,\mathrm{N/m}$ (Gurtin and Murdoch 1978). For such materials, the study in Lu et al. (2006) indicates that when a structure of thickness of micrometer order, the surface effect is pronounced. Thus we choose a microcantilever of diameter 8 μm and length 40 μm. From such a circular microcantilever, we examine the effect of these parameters on the force–frequency interaction curves.

4.1 Effect of residual surface tension

First, let us consider the effect of residual surface tension on the critical load for a microcantilever in a free space ($k = 0$) under a subtangential follower force. Figure 2a, b show the force–frequency interaction diagram between the dimensionless force p and dimensionless frequency Ω for a microcantilever subjected to a subtangential follower force with various tangency coefficients for $\eta = 0.391$, $\eta = 1.564$, respectively, where $\lambda = 0$ and $\mu = 0$ are imposed. In Fig. 2a, b, solid lines stand for the case of the presence of residual surface tension, while dashed lines for the case without residual surface tension, i.e. the classical case. Moreover, the curves marked with $\beta = 0$, corresponding to the case of a conservative force, consist of two separate lines (modes 1 and 2), and in this case, when $p = 0$ two curves intersect the Ω-axis at two distinct positions with and without the surface effects, which are the first and second natural frequencies, respectively. Without the surface effect, we find the intersecting positions at the Ω-axis are $\Omega = 3.516$ and 22.035, identical to the fundamental and second natural frequencies of a cantilever (Weaver et al. 1990). When the surface residual tension is taken into account, the natural frequencies become larger as if the cantilever is pulled tightly.

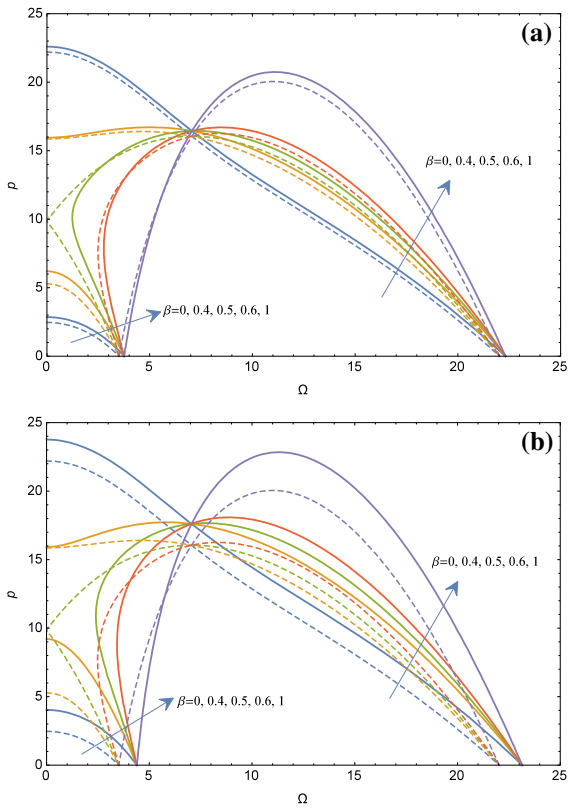

Fig. 2 Force–frequency interaction diagram between the dimensionless force p and dimensionless frequency Ω for a microcantilever subjected to a subtangential follower force with residual surface tension and without surface elasticity and surface mass ($\lambda = 0, \mu = 0$), **a** $\eta = 0.391$, **b** $\eta = 1.564$

Similarly, when $\Omega = 0$ these two curves intersect the p-axis at two positions, the lower one of which corresponds to the buckling load and the greater one corresponds to the second divergence force. In particular, the lower intersecting point at the p-axis of the curve of $\beta = 0$ gives the buckling load $p = 2.467$ for $\beta = 0$, agreeing with the well-known buckling load $\pi^2/4$ of a cantilever (Simitses and Hodges 2006). With the tangency coefficient β rising, the force–frequency interaction curve of mode 1 changes to lie above that of mode 1 for $\beta = 0$, whereas that of mode 2 decreases to lie below that of mode 2 for $\beta = 0$. Both curves of modes 1 and 2 tend to be closer and closer when β is further raised. Finally, both curves coalesce to become a constinuous curve. For example, for the classical case, the force–frequency curves of modes 1 and 2 intersect at the p-axis at two distinct positions for $\beta < 0.5$, both of which decrease with Ω rising, meet at the same position of the p-axis for $\beta = 0.5$, and have no intersecting position at the p-axis but coalesce to a curve when $\beta \geq 0.5$. Moreover, for $\beta > 0.5$, the force–frequency interaction curve has a highest position at a nonvanishing Ω value, which gives a flutter load. As a result, for a subtangential follower force or partially follower force with small tangency

coefficients $\beta < 0.5$, flutter instability does not take place, and only divergence instability such as buckling occurs. For a subtangential follower force or partially follower force with large tangency coefficients $\beta \geq 0.5$, flutter instability takes place, but buckling does not occur. This is possible due to greater contribution of the vertical component of the follower force than the horizontal component. When the residual surface tension is taken into account, by comparing Fig. 2a with 2b, we find that residual surface tension has a remarkable effect on the force–frequency interaction curves, in particular for those with β close to 0.5. From Fig. 2b, the value of β across which the force–frequency curves of mode 1 and 2 coalesce at the p-axis becomes slightly lower. Since Fig. 2a, b correspond to $L = 5d$ and $L = 10d$, for the same residual surface tension, the larger the slenderness ratio, the more remarkable the surface effects. In other words, for a longer elastic microcantilever when surface residual tension is taken into account, the dimensionless buckling load, flutter load, and fundamental frequency all become larger. It is noted that the force–frequency interaction curves for $\beta > 1$ are also possible in practice and they are not displayed in Fig. 2.

As we know, the divergence-type instability refers to a structure transiting from stability to instability at zero frequency, whereas the flutter instability refers to a structure passing from stability to instability through a dynamic process at a nonvanishing frequency. The values of force–frequency interaction curves when $\Omega = 0$ are called divergence forces and depend on β. The divergence force of the first-order mode for a conservative force $\beta = 0$ corresponds to the well-known Euler buckling loading. Clearly, when $\beta < 0.5$ without residual surface tension, the divergence force takes two different values, while when $\beta > 0.5$, $\beta = 1$, say, the force–frequency interaction curve has no intersecting point with the vertical axis. In this case, flutter instability occurs and the highest position of each force–frequency curve gives the corresponding critical flutter load. When considering surface stress, the force–frequency interaction curve has a similar trend. For a conservative force with $\beta = 0$, from Fig. 2a, b we see that the effect is stronger for the first-order mode than for the second-order or higher modes. It is interesting to note that all solid curves or dashed lines have common intersecting points at the frequency axis for different β values. This is easily understood since these positions correspond to the natural frequencies in the absence of axial loading. When residual surface tension is considered, the natural frequencies have a bit difference. Besides the above-mentioned common intersecting points at the frequency axis, there are still a notable characteristic. That is, all solid curves intersect at a position about $(\Omega, p) = (7.1, 16.4)$ in Fig. 2a and $(\Omega, p) = (7.1, 17.6)$ in Fig. 2b, likely all dashed curves also intersect at a position $(\Omega, p) = (7.05, 16.1)$. Obviously, these intersecting points are independent of β, but depend on η values. In fact, this intersecting point corresponds to the lowest one among flutter loads for a generalized follower force with arbitrary tangency coefficient, as explained in Li et al. (2016). Since the highest position having nonvanishing frequency value Ω of the force–frequency interaction curve implies occurrence of flutter instability, which gives flutter load, from Fig. 2a, b, the flutter instability is affected by the residual surface tension. For clarity, Fig. 3 show the stability boundary map against the tangency coefficient β for a microcantilever subjected to a subtangential follower force.

4.2 Effect of surface elasticity

Now we examine the effect of surface elasticity on dynamic stability of a microcantilever subjected to a subtangential follower force. In this case, we take $\lambda = 0.351$, $\mu = 0$ and $\eta = 0$, i.e. the residual surface tension and surface mass are neglected. Fig. 4 give a comparison of force–frequency interaction diagram

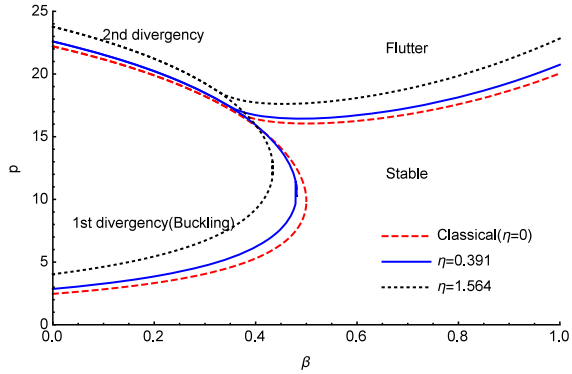

Fig. 3 Comparison of the stability boundary map showing the critical load as a function of the tangency coefficient β for a microcantilever subjected to a subtangential follower force with residual surface tension and without surface elasticity and surface mass ($\lambda = 0, \mu = 0$)

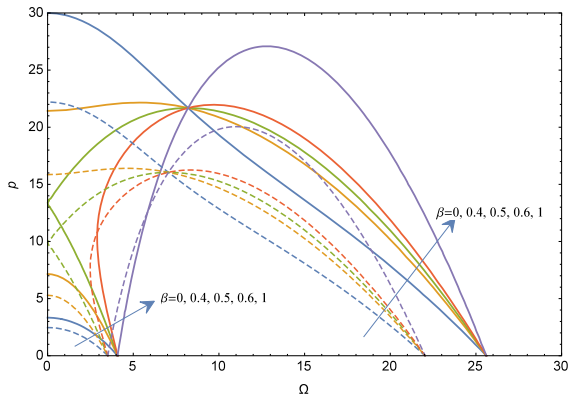

Fig. 4 Force–frequency interaction diagram between the dimensionless force p and dimensionless frequency Ω for a microcantilever subjected to a subtangential follower force with surface elasticity and without residual surface tension and surface mass $(\lambda = 0.351, \eta = 0, \mu = 0)$

when considering or neglecting the surface elasticity. Obviously, the change in the surface elasticity gives rise to a pronounced response of the force–frequency interaction curves. A positive surface elastic modulus increases the critical buckling or flutter load since the force–frequency interaction curve is always above the corresponding classical interaction curve, as seen in Fig. 4. For this case, we find that coalescence tangency coefficient does not change and is still $\beta = 0.5$; however, the critical buckling load has an apparent change. Fig. 4 only gives the numerical results of a positive surface elasticity. The trend for a negative surface elasticity is completely opposite to that observed in Fig. 4 and is not presented.

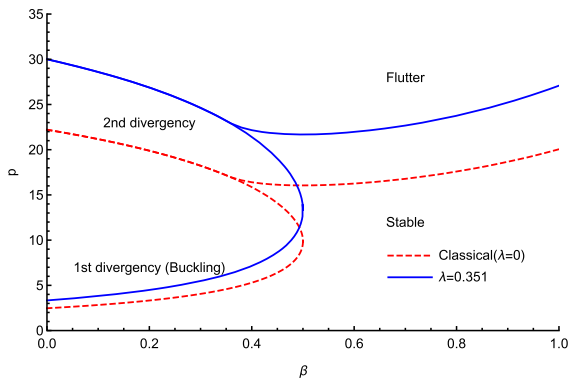

Fig. 5 Comparison of the stability boundary map showing the critical load as a function of the tangency coefficient β for a microcantilever subjected to a subtangential follower force with surface elasticity and without residual surface tension and surface mass $(\lambda = 0.351, \eta = 0, \mu = 0)$

Also, Fig. 5 depicts the critical loading p as a function of the tangency coefficient β for a microcantilever with surface elasticity subjected to a subtangential follower force without residual surface tension and surface mass. In Fig. 5, solid line corresponds to the case of consideration of surface elasticity, and dashed line to the case without surface elasticity. Clearly, not only buckling load but also flutter load have an increase as compared to the classical counterparts.

4.3 Effect of surface mass

Here we examine the effect of surface mass on dynamic stability of a microcantilever subjected to a subtangential follower force. In this case, we take $\mu = 0.117$, $\lambda = 0$ and $\eta = 0$, i.e. the residual surface tension and surface elasticity are neglected. Fig. 6 displays the force–frequency interaction diagram when considering or neglecting the surface mass, corresponding to solid lines or dashed lines, respectively. In this case, it is found that solid and dashed lines with the same tangency coefficient have a common intersecting position with the vertical p-axis, which implies that surface mass does not change the Euler buckling loading or divergency load. Furthermore, when the frequency becomes large, there is an apparent difference between solid and dashed lines for the same β values. However, solid and dashed force–frequency interaction curves with the same β values have the identical maximum value. This is to say that

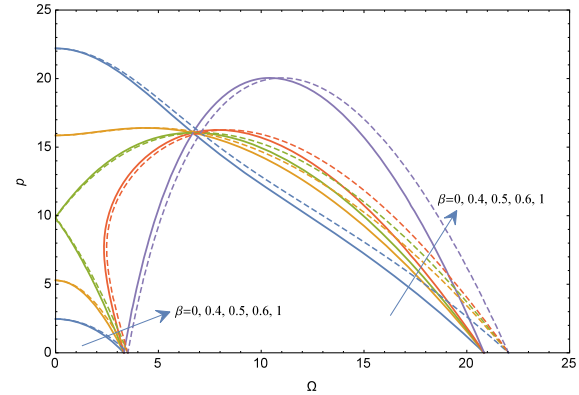

Fig. 6 Force–frequency interaction diagram between the dimensionless force p and dimensionless frequency Ω for a microcantilever subjected to a subtangential follower force with surface mass $\mu = 0.117$ and without surface elasticity and residual surface tension $(\lambda = 0, \eta = 0)$

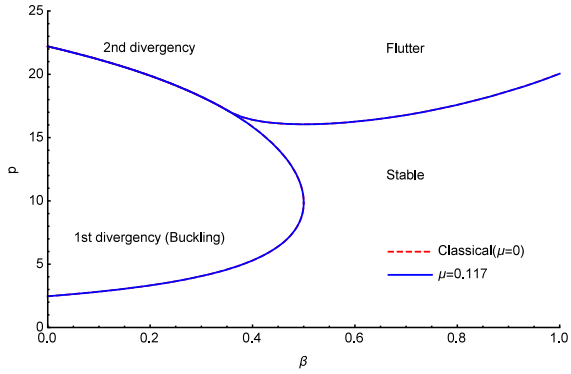

Fig. 7 Comparison of the stability boundary map showing the critical load as a function of the tangency coefficient β for a microcantilever subjected to a subtangential follower force with surface mass $\mu = 0.117$ and without surface elasticity and residual surface tension $(\lambda = 0, \eta = 0)$

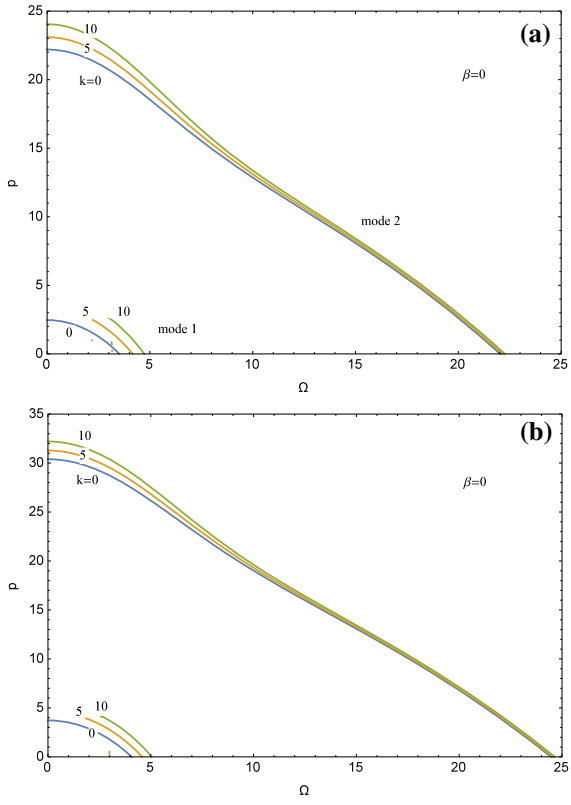

Fig. 8 Force–frequency interaction diagram between the dimensionless force p and dimensionless frequency Ω for a microcantilever on an elastic foundation or embedded in an elastic medium under a conservative force $(\beta = 0)$ at the free end, **a** the classical case, **b** the surface effect included $(\lambda = 0.351, \mu = 0.117, \eta = 0.391)$

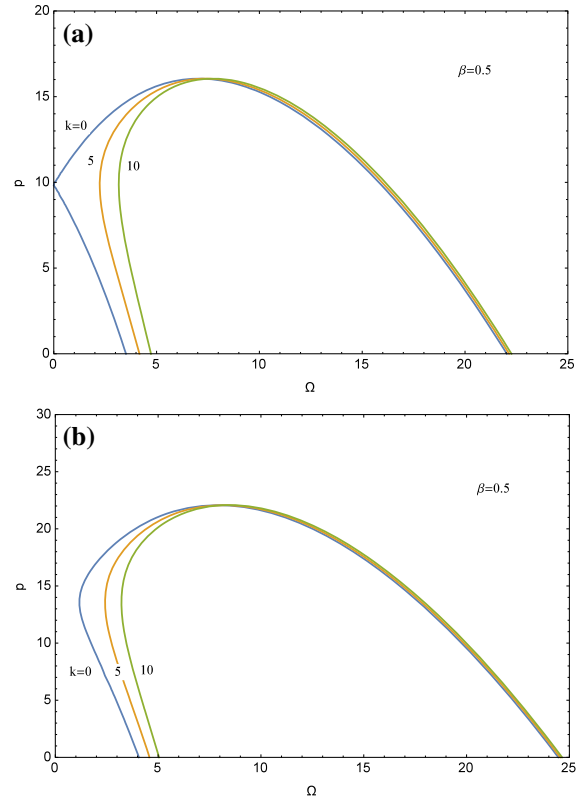

Fig. 9 Force–frequency interaction diagram between the dimensionless force p and dimensionless frequency Ω for a microcantilever on an elastic foundation or embedded in an elastic medium under a subtangential follower force $(\beta = 0.5)$ at the free end, **a** the classical case, **b** the surface effect included $(\lambda = 0.351, \mu = 0.117, \eta = 0.391)$

the stability boundaries are not sensitive to the surface mass, although the force–frequency interaction is affected. This is easily viewed from Fig. 7, which shows the complete overlap of two stability boundaries. In Fig. 7, dashed and dotted lines standing for the case of surface mass included and excluded, respectively completely coincide.

4.4 Effect of elastic foundation

In the above discussion, a microcantilever is placed in a free space. Sometimes, microcantilevers are placed sufficiently close to or rest on an elastic foundation, and the interaction between the microcantilever and the elastic foundation needs considering. In order to assess the influence of elastic foundation, we choose the same material with $\lambda = 0.351, \mu = 0.117, \eta =$

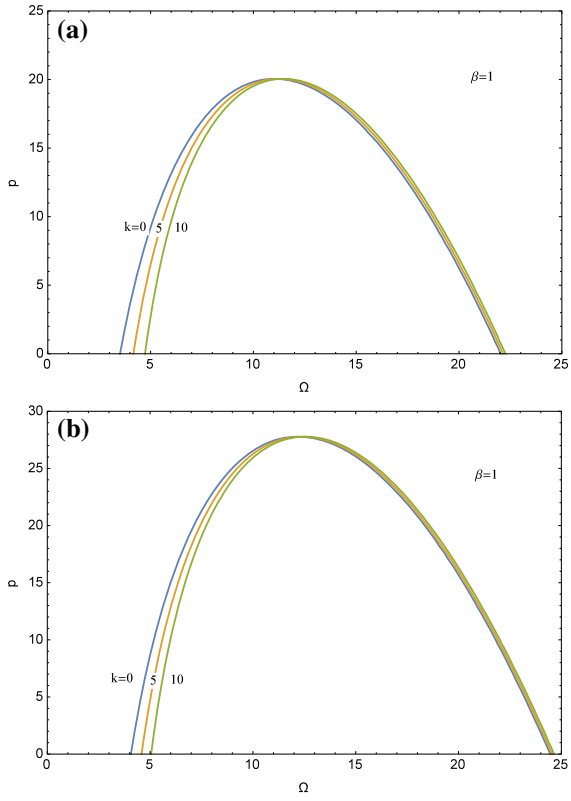

Fig. 10 Force–frequency interaction diagram between the dimensionless force p and dimensionless frequency Ω for a microcantilever on an elastic foundation or embedded in an elastic medium under a follower force ($\beta = 1$) at the free end, **a** the classical case, **b** the surface effect included ($\lambda = 0.351, \mu = 0.117, \eta = 0.391$)

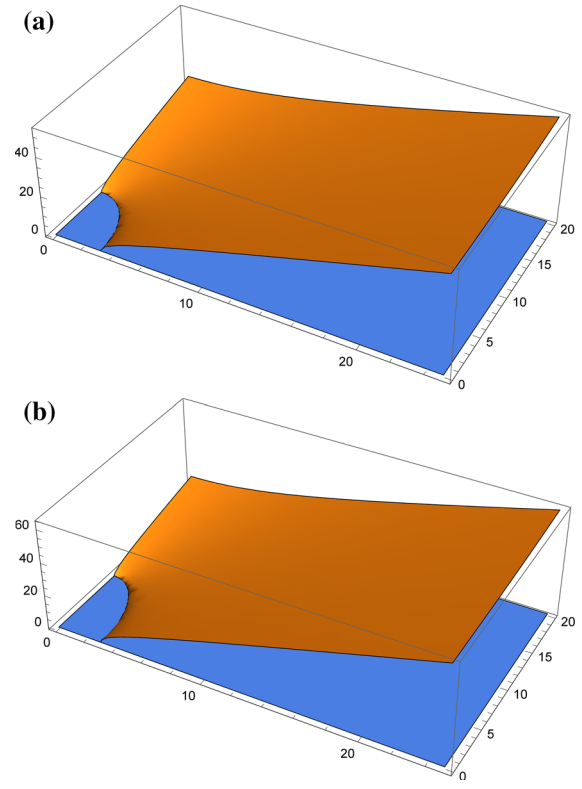

Fig. 11 The range of the parameter $\sqrt{\zeta}(\zeta > 0)$ against Ω and p for a microcantilever on elastic foundation, **a** the classical case without the surface effect, **b** the surface effect is considered ($\lambda = 0.351, \mu = 0.117, \eta = 0.391$)

0.391. For convenience, it is assumed that the dimensionless stiffness k satisfies $k < (p-\eta)^2/4(1+\lambda) + (1+\mu)\Omega^2$, which means that applied loading or vibration frequency is large enough to that the cantilever vibrates or even loss of stability takes place. Under such a circumstance, we give a comparison of force–frequency interaction diagram between the dimensionless force p and dimensionless frequency Ω for a microcantilever on an elastic foundation when subjected to a force at the free end with and without the surface effect in Figs. 8, 9 and 10. Note that $\beta = 0$ corresponds to the case of a conservative force, while $\beta = 1$ to the case of a follower force. For other β values, we only depict force–frequency interaction diagram for $\beta = 0.5$. From Fig. 8a, b, one can find that when considering the surface effect, the stiffness of the elastic foundation clearly affects the critical divergency force. Moreover, the influence on the divergency force is greater than that on the natural frequencies. It is worth noting that the force–frequency interaction curves corresponding to $k = 5$ and 10 for mode 1 do not meet the p-axis, while that to $k = 0$ meets the p-axis. The reason is that such k values violate the above-mentioned assumption. In other words, a necessary condition of harmonic vibration of a microcantilever is that $\zeta > 0$ in (24), where $\zeta = (p-\eta)^2 + 4(1+\lambda)\left[(1+\mu)\Omega^2 - k\right]$. Figure 11a, b depict the positive part of $\sqrt{\zeta}(\zeta > 0)$ as a function of Ω and p in the case of $k = 10$ without and with the surface effect. Obviously, when p and Ω become very low simultaneously, a positive k value leads to $\zeta < 0$, which implies no harmonic vibration. It is interesting to point out that the range of the domain satisfying $\zeta > 0$ is neither related end constraint nor applied load along with tangency coefficient, it only depends on the microcantilever itself as well as the elastic foundation. This is a necessary condition for harmonic

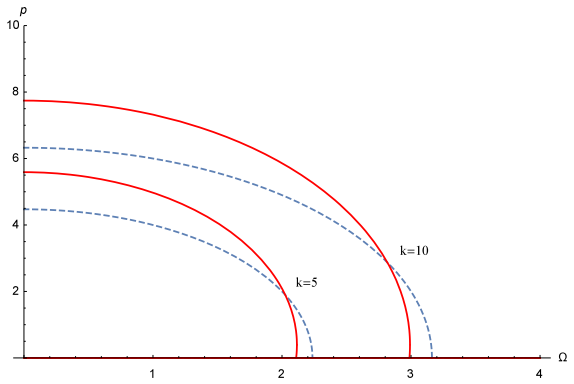

Fig. 12 The boundary of reasonable p and Ω values for different values of k, *solid lines* with surface effect, *dashed lines* without surface effect

vibrating occurring. As a result, for $k > 0$, p and Ω must satisfy some conditions such that a microcantilever to vibrate. For clarity, Fig. 12 shows the boundary of reasonable p and Ω values for two different values of k. The domain below solid lines for the surface effect included and dashed lines for the classical case with the surface effect indicates a range of (Ω, p) in which no harmonic vibration occurs. This also implies that for a microcantilever in a free space, there exist a buckling load, i.e. the first-order divergency force. For a microcantilever on an elastic foundation with larger value of k, the force to lead to loss of stability is raised to be larger than 22 in Fig. 8a and $p > 30$ in Fig. 8b, which in fact nearly corresponds to the second-order divergency force of $k = 0$. Although the elastic foundation changes the divergency force, but does not affect the flutter load, which can be seen from Figs. 9 and 10 since all curves intersect at the highest position. Therefore, an elastic foundation affects the divergency force, but does not affect flutter load.

5 Conclusions

In this paper, dynamic stability of microcantilevers subjected to a generalized follower force was dealt with when the surface effects were taken into account. By solving the corresponding boundary value problem, an exact characteristic equation was derived. The force–frequency interaction was presented graphically for various interesting cases. Divergence and flutter loads were given for any tangency coefficient. Buckling load for a conservative compressive force was recovered from vanishing tangency coefficient. Some conclusions are drawn as follows:

- Flutter instability occurs for some subtangential follower forces with tangency coefficients larger than a certain value.
- Positive surface elastic modulus increases the divergence or flutter load, and negative one decreases the divergence or flutter load.
- Residual surface tension gives rise to the increase of divergence or flutter load. The influence is more noticeable for slender microcantilevers.
- Surface mass does not change the divergence or flutter load, but affect the natural frequencies of microcantilevers.
- An elastic foundation affects the divergency force, but does not affect flutter load.

Acknowledgements This work was supported by the National Natural Science Foundation of China (No. 11672336) and the Open Foundation of State Key Laboratory of Structural Analysis for Industrial Equipment, Dalian University of Technology, PRC (No. GZ15204).

References

Agwa, M.A., Eltaher, M.A.: Vibration of a carbyne nanomechanical mass sensor with surface effect. Appl. Phys. A **122**, 335 (2016)

Ansari, R., Mohammadi, V., Shojaei, M.F., Gholami, R., Rouhi, H.: Nonlinear vibration analysis of Timoshenko nanobeams based on surface stress elasticity theory. Eur. J. Mech. A Solids **45**, 143–152 (2014)

Attia, M.A., Mahmoud, F.F.: Modeling and analysis of nanobeams based on nonlocal-couple stress elasticity and surface energy theories. Int. J. Mech. Sci. **105**, 126–134 (2016)

Chen, T.Y., Chiu, M.S.: Effects of higher-order interface stresses on the elastic states of two-dimensional composites. Mech. Mater. **43**, 212–221 (2011)

Chen, X., Meguid, S.A.: Asymmetric bifurcation of initially curved nanobeam. J. Appl. Mech. **82**, 091003 (2015a)

Chen, X., Meguid, S.A.: On the parameters which govern the symmetric snap-through buckling behavior of an initially curved microbeam. Int. J. Solids Struct. **66**, 77–87 (2015b)

Chen, X., Meguid, S.A.: Snap-through buckling of initially curved microbeam subject to an electrostatic force. Proc. R. Soc. A **471**, 20150072 (2015c)

Chen, X., Meguid, S.A.: Asymmetric bifurcation of thermally and electrically actuated functionally graded material microbeam. Proc. R. Soc. A **472**, 20150597 (2016)

Chiu, M.S., Chen, T.Y.: Effects of high-order surface stress on buckling and resonance behavior of nanowires. Acta Mech. **223**, 1473–1484 (2012)

Chiu, M.S., Chen, T.Y.: Bending and resonance behavior of nanowires based on Timoshenko beam theory with high-order surface stress effects. Phys. E **54**, 149–156 (2013)

Cuenot, S., Fretigny, C., Demoustier-Champagne, S., Nysten, B.: Surface tension effect on the mechanical properties of nanomaterials measured by atomic force microscopy. Phys. Rev. B **69**, 165410 (2004)

Dingreville, R., Qu, J., Cherkaoui, M.: Surface free energy and its effect on the elastic behavior of nano-sized particles, wires and films. J. Mech. Phys. Solids. **53**, 1827–1854 (2005)

Dorignac, J., Kalinowski, A., Erramilli, S., Mohanty, P.: Dynamical response of nanomechanical oscillators in immiscible viscous fluid for in vitro biomolecular recognition. Phys. Rev. Lett. **96**, 186105 (2006)

Elishakoff, I., Soret, C.: A consistent set of nonlocal Bresse–Timoshenko equations for nanobeams with surface effects. J. Appl. Mech. **80**, 061001 (2013)

Farshi, B., Assadi, A., Alinia-ziazi, A.: Frequency analysis of nanotubes with consideration of surface effects. Appl. Phys. Lett. **96**, 093105 (2010)

Gao, X.L.: A new Timoshenko beam model incorporating microstructure and surface energy effects. Acta Mech. **226**, 457–474 (2015)

Gavan, K.B., Westra, H.J.R., van der Drift, E.W.J.M., Venstra, W.J., van der Zant, H.S.J.: Size-dependent effective Young's modulus of silicon nitride cantilevers. Appl. Phys. Lett. **94**, 233108 (2009)

Gurtin, M.E., Murdoch, A.I.: A continuum theory of elastic material surfaces. Arch. Ration. Mech. Anal. **57**, 291–323 (1975)

Gurtin, M.E., Murdoch, A.I.: Surface stress in solids. Int. J. Solids Struct. **14**, 431–440 (1978)

He, J., Lilley, C.M.: Surface stress effect on bending resonance of nanowires with different boundary conditions. Appl. Phys. Lett. **93**, 263108 (2008a)

He, J., Lilley, C.M.: Surface effect on the elastic behavior of static bending nanowires. Nano Lett. **8**, 1798–1802 (2008b)

He, Q.L., Lilley, C.M.: Resonant frequency analysis of Timoshenko nanowires with surface stress for different boundary conditions. J. Appl. Phys. **112**, 074322 (2012)

Hosseini-Hashemi, S., Nazemnezhad, R., Rokni, H.: Nonlocal nonlinear free vibration of nanobeams with surface effects. Eur. J. Mech. A. Solids. **52**, 44–53 (2015)

Kiani, K.: Forced vibrations of a current-carrying nanowire in a longitudinal magnetic field accounting for both surface energy and size effects. Phys. E. **63**, 27–35 (2014)

Kiani, K.: Axial buckling analysis of a slender current-carrying nanowire acted upon by a magnetic field using the surface energy approach. J. Phys. D Appl. Phys. **48**, 245302 (2015)

Lachut, M.J., Sader, J.E.: Effect of surface stress on the stiffness of cantilever plates. Phys. Rev. Lett. **99**, 206102 (2007)

Lee, H.L., Chang, W.J.: Surface effects on frequency analysis of nanotubes using nonlocal Timoshenko beam theory. J. Appl. Phys. **108**, 093503 (2010)

Li, X.-F., Peng, X.-L.: Theoretical analysis of surface stress for a microcantilever with varying widths. J. Phys. D Appl. Phys. **41**, 065301 (2008)

Li, X.-F., Zhang, H., Lee, K.Y.: Dependence of Young's modulus of nanowires on surface effect. Int. J. Mech. Sci. **81**, 120–125 (2014)

Li, X.F., Zou, J., Jiang, S.N., Lee, K.Y.: Resonant frequency and flutter instability of a nanocantilever with the surface effects. Compos. Struct. **153**, 645–653 (2016)

Liu, C., Rajapakse, R.: Continuum models incorporating surface energy for static and dynamic response of nanoscale beams. IEEE Trans. Nanotechnol. **9**, 422–431 (2010)

Lu, P., He, L.H., Lee, H.P., Lu, C.: Thin plate theory including surface effects. Int. J. Solids Struct. **43**, 4631–4647 (2006)

McFarland, A.W., Poggi, M.A., Doyle, M.J., Bottomley, L.A., Colton, J.S.: Influence of surface stress on the resonance behavior of microcantilevers. Appl. Phys. Lett. **87**, 53505–53505 (2005)

Miller, R.E., Shenoy, V.B.: Size-dependent elastic properties of nanosized structural elements. Nanotechnology **11**, 139 (2000)

Nazemnezhad, R., Hosseini-Hashemi, S.: Nonlinear free vibration analysis of Timoshenko nanobeams with surface energy. Meccanica **50**, 1027–1044 (2015)

Qiao, L., Zheng, X.J.: Effect of surface stress on the stiffness of micro/nanocantilevers: nanowire elastic modulus measured by nano-scale tensile and vibrational techniques. J. Appl. Phys. **113**, 013508 (2013)

Shenoy, V.B.: Atomistic calculations of elastic properties of metallic fcc crystal surfaces. Phys. Rev. B **71**, 094104 (2005)

Simitses, G.J., Hodges, D.H.: Fundamentals of Structural Stability. Butterworth-Heinemann, London (2006)

Wang, L.: Vibration analysis of fluid-conveying nanotubes with consideration of surface effects. Phys. E. **43**, 437–439 (2010)

Wang, G.-F., Feng, X.-Q.: Effects of surface elasticity and residual surface tension on the natural frequency of microbeams. Appl. Phys. Lett. **90**, 231904 (2007)

Wang, G.-F., Feng, X.-Q.: Timoshenko beam model for buckling and vibration of nanowires with surface effects. J. Phys. D Appl. Phys. **42**, 155411 (2009)

Wang, J., Huang, Z., Duan, H., Yu, S., Feng, X., Wang, G., Zhang, W., Wang, T.: Surface stress effect in mechanics of nanostructured materials. Acta Mech. Solid Sin. **24**, 52–82 (2011)

Wang, H., Li, X., Tang, G., Shen, Z.: Effect of surface stress on stress intensity factors of a nanoscale crack via double cantilever beam model. J. Nanosci. Nanotechnol. **13**, 477–482 (2013)

Wang, K.F., Wang, B.L.: A general model for nano-cantilever switches with consideration of surface effects and nonlinear curvature. Phys. E. **66**, 197–208 (2015)

Weaver Jr., W., Timoshenko, S.P., Young, D.H.: Vibration Problems in Engineering. Wiley, New York (1990)

Wu, J.-X., Li, X.-F., Tang, A.-Y., Lee, K.Y.: Free and forced transverse vibration of nanowires with surface effects. J. Vib. Control. 1077546315610302 (2016)

Yi, X., Duan, H.L.: Surface stress induced by interactions of adsorbates and its effect on deformation and frequency of microcantilever sensors. J. Mech. Phys. Solids. **57**, 1254–1266 (2009)

Zhang, J., Meguid, S.A.: Effect of surface energy on the dynamic response and instability of fluid-conveying nanobeams. Eur. J. Mech. A Solids. **58**, 1–9 (2016)

Zhang, Y.Q., Pang, M., Chen, W.Q.: Transverse vibrations of embedded nanowires under axial compression with high-order surface stress effects. Phys. E. **66**, 238–244 (2015)

Zhang, Y., Ren, Q., Zhao, Y.-P.: Modelling analysis of surface stress on a rectangular cantilever beam. J. Phys. D Appl Phys. **37**, 2140 (2004)

Zheng, X.P., Cao, Y.P., Li, B., Feng, X.Q., Wang, G.F.: Surface effects in various bending-based test methods for measuring the elastic property of nanowires. Nanotechnology **21**, 205702 (2010)

Zuo, Q.H., Schreyer, H.L.: Flutter and divergence instability of nonconservative beams and plates. Int. J. Solids Struct. **33**, 1355–1367 (1996)